



Sintering of 3D-printed aluminum specimens from the slurry-based binder jetting process

Jan Angenoorth^{1,2} · Patricia Erhard¹ · Dennis Wächter² · Wolfram Volk^{1,2} · Daniel Günther¹

Received: 26 April 2024 / Accepted: 7 May 2024 / Published online: 17 May 2024
© The Author(s) 2024

Abstract

This work investigates a novel method of producing complex-shaped aluminum parts by slurry-based binder jetting and sintering. In this process, a green body is built up by layer-wise deposition of an aqueous aluminum suspension and selective powder bonding by ink-jet printing. The powder bulk generated from the suspension shows an increased density compared to powder-based binder jetting and, thus, a high initial density for the subsequent densification step. This allows for higher final densities and reduced shrinkage. Aluminum is of special interest as it is widely available and of low density but challenging to sinter due to an oxide skin surrounding every particle. The research in this paper investigates the effects of the sintering atmosphere and sintering additives on the microstructure of powder compacts produced by slurry-based binder jetting. The incorporation of magnesium as an additive during the sintering process of aluminum has been found to substantially improve densification during sintering in an argon atmosphere.

Keywords Additive manufacturing · Binder jetting · Aluminum · Slurry-based binder jetting

1 Introduction and motivation

ISO/ATSM 52900 defines additive manufacturing (AM) as a technique for creating shapes directly from 3D data, which differs from alternative subtractive and formative methods by building layer upon layer. The binder jetting AM technique involves layering powder materials and printing onto layers with a binder. This method was developed by Sachs originally to print molds to be used in metal casting [1]. The limited powder flowability of small particle sizes resulted in low density, stability, and poor surface quality of dryly built parts. This constraint was found to restrict the area of application. Sachs later proposed a solution to this issue by explicitly describing the layer-wise deposition of fine powders dispersed in a liquid in a second patent [2]. Using fine particle suspensions instead of dry powders increases the achievable packing density. Full densification can be achieved in a subsequent sintering step [3, 4].

Due to several challenges, aluminum has only limited representation in the field of AM. These include poor weldability due to the stable oxide layer and high reflectivity in the laser wavelengths typically used. Furthermore, aluminum is easily machinable, which enables rapid and cost-effective production with conventional methods, reducing the economic value of AM [5]. However, it makes sense to use AM processes for highly complex 3D components.

The binder jetting process involves the following repeated steps: first, a build platform is lowered by the desired layer thickness. Then, the free volume is filled with powder by a coating mechanism. Next, the powder is selectively printed with a binder in the corresponding layer. This represents the geometry of the respective cross-section and creates a connection to the previous layer. After completing the layer-by-layer structure, the printed parts supported by the surrounding powder may be cured depending on the binder type. Then, the loose powder is removed from the components. The printed, porous components may be subjected to a post-processing step, in which they are sintered or infiltrated to reach their final properties [6]. The processability of powders in a dry state is limited to particle diameters $\geq 20 \mu\text{m}$ due to the required flowability in the binder jetting process [7]. However, finer powders $< 20 \mu\text{m}$ have larger surface

✉ Jan Angenoorth
jan.angenoorth@igcv.fraunhofer.de

¹ Fraunhofer IGC, Garching, Germany

² Technical University of Munich, Garching, Germany

areas and thus a higher energetic state, which enables faster compaction during sintering [6].

In slurry-based 3D printing, the powder is applied layer by layer as an environmentally friendly aqueous suspension, dried, and printed on. The achievable packing density is higher in this process alternative not only due to the fineness of the powder to be processed but also to the compaction via capillary forces during the dewatering of the respective layer through underlying layers. Higher packing densities minimize sintering shrinkage [6, 8] and are thus desirable in most applications. Slurry-based binder jetting has already been applied to ceramics. Packing densities of 50–60% of theoretical density could be achieved [4, 9]. Studies show that these green densities can achieve complete compaction after sintering [3, 4].

During sintering, particles are fused together to form a solid body through a diffusion-based process starting from a powder state. Powder metallurgy has a significant advantage over conventional methods in that it can work with a wide variety of materials and material combinations and influence their microstructure selectively.

The successful sintering of aluminum-based materials requires the removal or break-up of the oxide layer that covers the aluminum particles. This oxide skin prevents the connection of metal-to-metal contacts between adjacent powder particles necessary for sintering. The overall average oxide thickness of rapidly solidified powders of pure aluminum after exposure to a humid atmosphere was found to be around 5.5 nm [10]. The oxide layer Al_2O_3 surrounding the aluminum particles makes sintering aluminum powders difficult due to its stability. At 600 °C, an oxygen partial pressure of 10^{-22} bar [11] would be necessary to reduce this oxide skin. In addition, in the presence of oxygen in the sintering atmosphere (i.e., due to contamination of the protective gas), the oxide layer thickness even increases at higher temperatures [12]. This reduces the oxygen partial pressure in the protective gas as it penetrates the interior of the specimens through the interconnected pores. Although the outer layers of the samples are more strongly oxidized, the oxygen partial pressure inside the sintered body is lowered to the extent that sintering conditions are enabled. This effect is referred to as “self-gettering” [13]. The surface layer of the sintered body binds the oxygen remaining in the protective gas as impurities in favor of the core region. In the sintering of aluminum components, the oxide layer is, therefore, broken up by mechanical forces and/or chemically during the pressing of the green bodies [14]. Since neither of these methods is applied in the process under investigation, the oxide layer must be addressed in another way.

In the past, sintering has also been achieved by adjusting the sintering atmosphere [13, 15]. Studies have shown that a nitrogen atmosphere has a positive effect on the sintering process of aluminum [15]. It is believed that under a nitrogen

atmosphere, aluminum nitride (AlN) forms, which does not directly reduce the oxide layer [15]. It is assumed that an exothermic reaction of vaporized aluminum with nitrogen is a source of energy for local melting, allowing liquid aluminum to dissolve the oxide layer of other particles [15]. Furthermore, it is discussed if a reduction of the oxide layer by nitrogen can occur inside the sintered body [13].

Adding small amounts of magnesium (Mg) is another way to facilitate the sintering of aluminum. This can be done either by adding Mg to the powder or by providing it in the sintering furnace. According to Qian and Schaffer, Mg improves sintering behavior in two ways: it directly reduces the oxide layer, leading to sinterable elemental aluminum, and it lowers the oxygen partial pressure in the local sintering atmosphere by reacting with the oxygen in the protective gas [14]. However, the results varied depending on the alloy composition and powder purity, and there is no clear explanation for this. MacAskill et al. found that sintering can be improved, particularly by adding tin in addition to Mg, leading to liquid-phase sintering. In the experiments, a density of up to 99.5% of theoretical density was achieved [16].

Hydrogen is sometimes used to reduce oxide layers on metals [17]. However, according to Piczonka et al., even in low concentrations in a nitrogen atmosphere, hydrogen greatly reduces the sinterability of aluminum [18].

This study aims to investigate the effects of the sintering atmospheres nitrogen and argon and the sintering additive magnesium on the microstructure of powder compacts produced by the slurry-based 3D-printing process.

2 Materials and methods

2.1 Materials

The aqueous aluminum slurry used consists of 74 wt.-% aluminum powder (Rogal Aluminium 2/4, *Schlenk Metallic Pigments GmbH, Germany*; minimum purity of 99.7%, particle diameter $D_{50} = 5 \mu\text{m}$), 25.4 wt.-% deionized water, 0.3 wt.-% dispersant agent (Dolapix CE 64, *Zschimmer & Schwarz GmbH Co., Germany*), and 0.3 wt.-% thickening agent (Xanthan, *V03 Trading GmbH, Germany*). The slurry exhibits excellent stability and flowing behavior while showing no agglomeration and foaming.

Solid magnesium bodies (*HMW Hauner GmbH & Co. KG, Germany*) with a purity of 99.8% and a weight of $300 \text{ mg} \pm 30 \text{ mg}$ were used as a sintering additive in the sintering furnace.

2.2 Sample production

A binder jetting test rig, extensively used for the slurry-based binder jetting, was used to produce the investigated

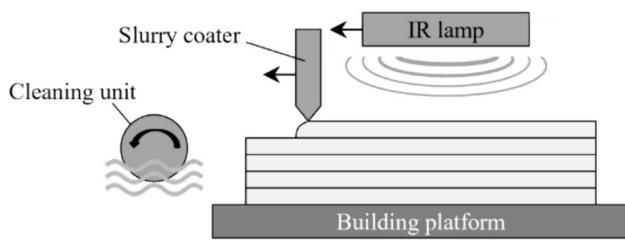


Fig. 1 Schematic representation of the slurry-based binder jetting process; adopted and expanded from Ref. [9]

powder compact. The slurry-based binder jetting experimental setup is composed of two fundamental modules, namely the coating module, which includes the building platform, the slurry coater, an infrared (IR) lamp and the cleaning unit; and the ink-jet printing module. For the purposes of this study, only the coating module was utilized that is depicted schematically in Fig. 1. The axis translation of the coating module is enabled by a linear actuator. The coater is fed by a pneumatically actuated slurry feeding system, which is responsible for depositing the metal slurry onto the building platform. The drying unit comprises an infrared lamp (IRD X230L, *Optron GmbH, Germany*) placed 65 mm above the laid layer that provides uniform heating at a radiated power density of 0.97 W/cm^2 on the deposited slurry layer during the drying process. To prevent slurry from drying and subsequently clogging the coater during the drying process of each layer, a cleaning unit comprising a continuously rotating roller immersed in water is strategically positioned so that the coater rests on the cleaning unit while each layer dries.

A powder compact with the approximate dimensions $60 \text{ mm} \times 30 \text{ mm} \times 6 \text{ mm}$ (length \times width \times height) and a layer thickness of $50 \mu\text{m}$ was built using the tests rig and the aluminum slurry. The powder compact was built on a porous substrate (MONALITE-M1T, *Etex Building Performance GmbH, Germany*) with excellent absorbency, and therefore, no IR drying was set for the first 10 layers. From the 11th layer, the drying time was set to 7.5 s. The coating velocity was 25 mm/s. The pre-load time, giving the period where the coater starts depositing slurry prior to movement, was set to 1.5 s.

Samples with the dimension of $5 \text{ mm} \times 5 \text{ mm} \times 5 \text{ mm}$ were cut from the powder compact and sintered in a subsequent process.

2.3 Sintering

A heating microscope (DIL L74 Optical Dilatometer, *Linseis Messgeräte GmbH, Germany*) was used for sintering the samples. A vacuum of approximately 10^{-4} hPa was generated using a vacuum pump (HiCube 80 eco, *Pfeiffer*

Vacuum GmbH, Germany) before flooding the furnace with protective gas at a constant gas pressure of 0.2 bar. Vacuum drawing and flooding were not performed when sintering in a normal atmosphere. The heating rate for the sintering process was set to 20 K/min and the target temperature was $600 \text{ }^\circ\text{C}$. After a 2-h holding time at a temperature of $600 \text{ }^\circ\text{C}$, the sintering furnace was cooled down to $100 \text{ }^\circ\text{C}$ at a cooling rate of 10 K/min. The cooling rate of 10 K/min could not be realized at temperatures below $400 \text{ }^\circ\text{C}$ due to the limited cooling capacity of the appliance. However, the temperature curve was constant for every sintering cycle investigated and the cooling rate should not have affected the microstructure further at those low temperatures. In Fig. 2, the temperature profile of the sintering process is shown. The dotted curve represents the ideal temperature profile as set in the control system, while the solid curve represents the actual temperature profile. The selected sintering temperature of $600 \text{ }^\circ\text{C}$ is also marked on the graph.

Before the sintering process, two magnesium pieces were placed in front and behind the sintered sample, respectively, to ensure the optimal effect caused by the gas flow. Two samples were sintered in a single sintering process.

Two samples each were sintered under nitrogen (A6 and A7), argon (B6 and B7) and normal atmosphere (A5 and B5). Two additional sets of experiments were dedicated to sintering two samples each under nitrogen (C6 and C7) and argon (D6 and D7) atmosphere with magnesium addition (placed 3 mm in front and behind the sample) in the sintering furnace. Table 1 shows the parameters varied within this study.

2.4 Material characterization

Before and after sintering, the absolute and relative green part density, based on the density of pure aluminum (2.7 g/cm^3), were determined by measuring the volume with a

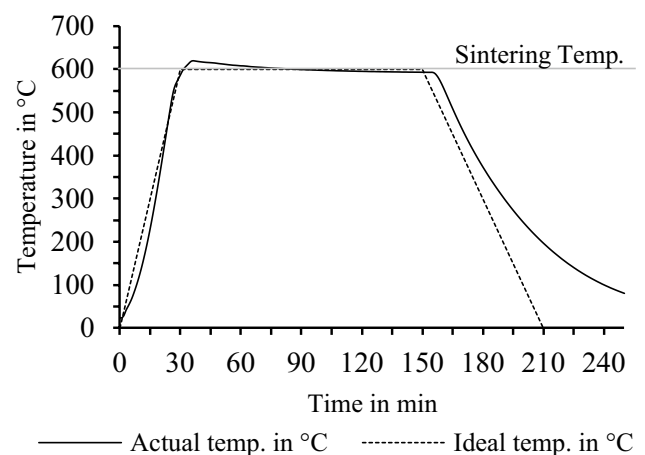


Fig. 2 Sintering temperature (temp.) profile

Table 1 Varied parameters in the sintering process

Specimens	Atmosphere	Magnesium
A6 and A7	N ₂	No
B6 and B7	Ar	No
C6 and C7	N ₂	Yes
D6 and D7	Ar	Yes
A5 and B5	Normal	No

micrometer and the weight with a scale (Secura 125–1S, Sartorius Lab Instruments GmbH & Co. KG, Germany). The values are given as relative densities ρ_{rel} , defined as

$$\rho_{rel} = \frac{\rho_{specimen}}{\rho_{aluminum}}$$

where $\rho_{specimen}$ is the density of each specimen, and $\rho_{aluminum}$ is the density of aluminum, being 2.7 g/cm³.

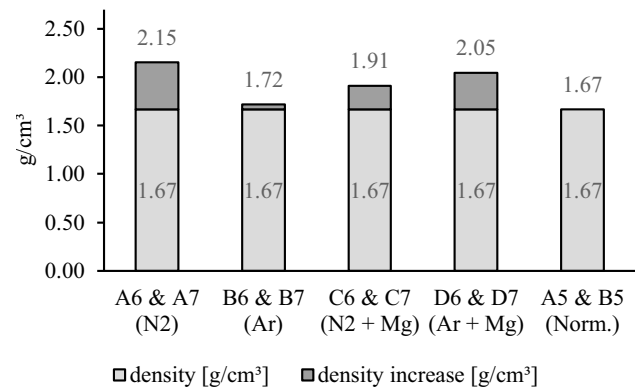
One sintered sample from each experimental series (A6, B7, D7, C6 and A5) is selected and evaluated in terms of uniformity and recognizable signs of successful sintering, such as density changes or sintering necks in metallographic examinations. A light microscope (BX53M, Olympus Europa SE & Co. KG, Germany) was used for the micrographs. For metallographic analysis, the sintered samples were embedded and polished to 0.1 μ m surface roughness.

Two selected sintered samples (A6 and D7) were analyzed with a scanning electron microscope (SEM) (TM3030Plus, Hitachi High-Techs Corp, Japan). This allows for an improved magnification regarding the topographical characteristics of the sintered samples.

3 Results and discussion

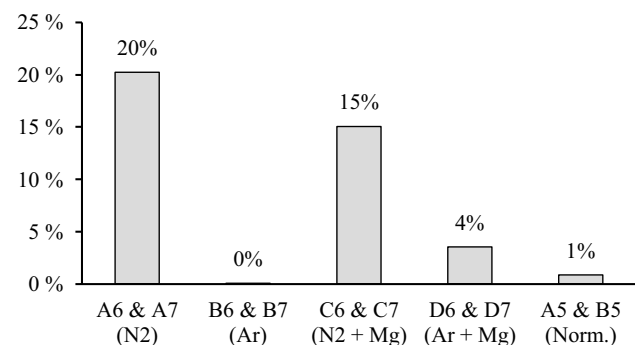
3.1 Density and mass

The density of the samples before sintering is 1.67 g/cm³. After sintering, the sample density varies depending on the sintering atmosphere and whether magnesium was added to the sintering furnace or not. The densities of the individual test series are shown in Fig. 3. The average density change of the two sintered samples A6 and A7 under nitrogen and without magnesium addition (N₂) shows the largest increase in density of 0.48 g/cm³. A significant increase in density of 0.38 g/cm³ is also noticeable in the samples D6 and D7 that were sintered under an argon protective gas atmosphere and with magnesium addition (Ar + Mg). The two samples C6 and C7 that were sintered under a nitrogen atmosphere and with magnesium addition (N₂ + Mg) show an increase in density of 0.24 g/cm³. The two samples B6 and B7, which were sintered under an argon atmosphere

**Fig. 3** Increase in density and overall density of the sintered samples

but without magnesium addition (Ar), show an increase in density of 0.05 g/cm³. The two samples A5 and B5, the only samples that were sintered under normal atmosphere and without magnesium addition (Norm.), showed no change in density during sintering.

Figure 4 shows the increase in mass during the sintering process under different protective gas atmospheres. Particularly noteworthy are the test series sintered under a nitrogen protective gas atmosphere, which exhibited the highest increase in mass. Samples A6 and A7, sintered under pure nitrogen atmosphere, showed an average mass increase of 20%. The relative density has increased from approximately 62% in the green specimens to 81% in the sintered specimens, related to the density of aluminum. The average mass of 239.0 g has increased by 48.4 g. The volume of the two specimens has decreased on average by 6.6%. The shrinkage of specimens A6 and A7 and the increase in relative density indicate a sintering process. The increase in mass indicates another reaction during the sintering process. This is most likely nitride formation due to the nitrogen sintering atmosphere. Nitrogen and aluminum react to form aluminum nitride AlN [14].

**Fig. 4** Increase in mass relative to the green body mass after the sintering process

Samples C6 and C7, sintered under a nitrogen atmosphere with the addition of magnesium in the sintering furnace, showed an average mass increase of 15%. This is probably due the formation of aluminum nitride [14].

3.2 Microstructure

One specimen from each series (A6, B7, C6, D7 and A5) was examined in detail under a light microscope.

The increase in density of samples A6 and A7 (Fig. 3), sintered under a nitrogen atmosphere, indicates a successful sintering process. This is further confirmed by the microscope images in Fig. 5. The microscope images b, c, and d in Fig. 5 of sample A6 do not show any individual aluminum particles, except in the outer shell (Fig. 5c). However, this can be explained by the “self-gettering” effect as explained above.

Looking at specimen B7 in Fig. 6, a clear outer layer can be seen that is similar to the thin outer layer of sample A6 (Fig. 5c). This is likely again because of “self-gettering”. The subsequent layer, which can also be seen in Fig. 6b and c, indicates a significant compression of this area and an advanced sintering process through deformation of the individual aluminum particles. Clear porosities can be seen inside of the sintered specimen. Specimens B6 and B7 shrunk an average of 3% and did not show any change in mass during the sintering process (Fig. 4s).

Specimens C6 and C7, which were sintered under a nitrogen atmosphere with an addition of magnesium in the sintering furnace, did not show any change in volume. However, the mass of the samples increased by 15%, which is probably due to nitride formation and the resulting aluminum nitride AlN. The inner area of specimen C6 looks very similar to the inner area of specimen A6. It is also noteworthy that sample C6, compared to A6, does not exhibit a “self-gettering” effect (compare Figs. 5c) and 7b). This is attributed to the addition of magnesium, which reduces the partial pressure of oxygen in the sintering atmosphere. The sample C6 is depicted in Fig. 7. When comparing the average mass gain of the sintered samples under a nitrogen atmosphere (A6 and A7) to the sintered samples under a nitrogen atmosphere with the addition of magnesium (C6 and C7), a discrepancy of 5% can be observed (Fig. 4). This may be due to the reaction of magnesium and nitrogen to form magnesium nitride (Mg_3N_2), resulting in less nitrogen being converted to aluminum nitride (AlN) in the aluminum samples C6 and C7. However, further investigation is needed to understand this phenomenon.

Specimens D6 and D7 showed a significant shrinkage of 16%, while the mass increased slightly by 4%. In Fig. 8a), the transition area, which is framed, is shown with an enlargement in b) and d). The density and sintering degree in the outer layer are significantly more advanced than in the inner area of the specimen. Sintering necks can be detected in the inner area. The SEM image in Fig. 8d) clearly shows

Fig. 5 **a** Microscope overview image of the sintered test specimen A6 (sintered under nitrogen); **b** detail image of the edge layer; **c** image of the unsintered outer layer; **d** SEM image

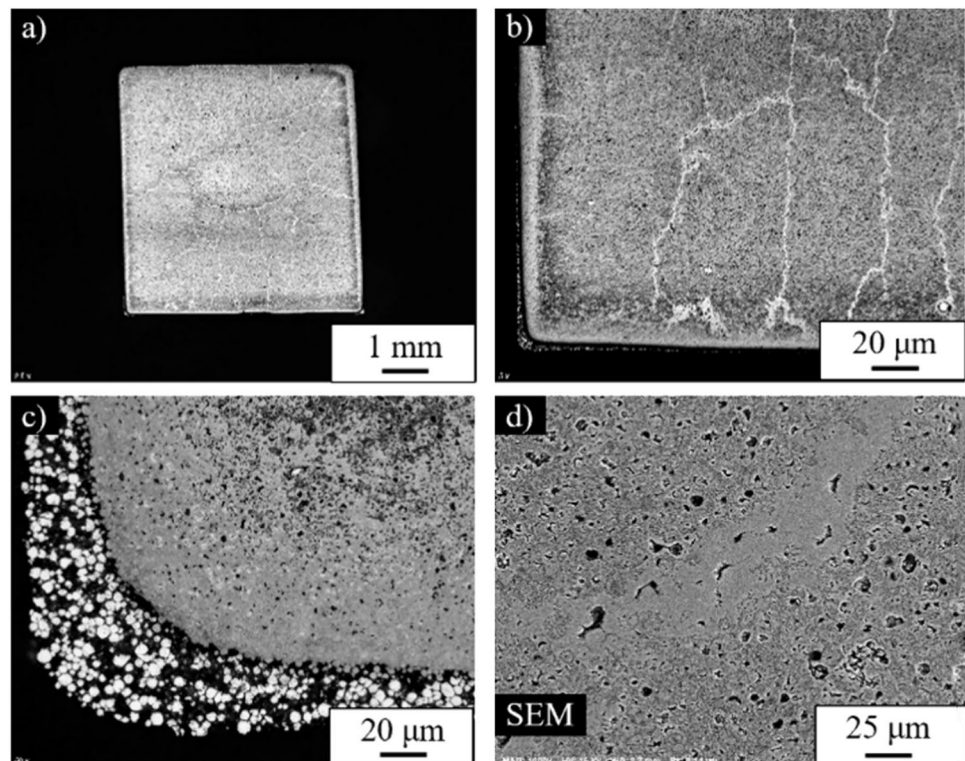


Fig. 6 **a** Microscope overview image of the sintered test specimen B7 (sintered under argon); **b** image of the transition zone between outer and inner area; **c** image of the sintered inner area

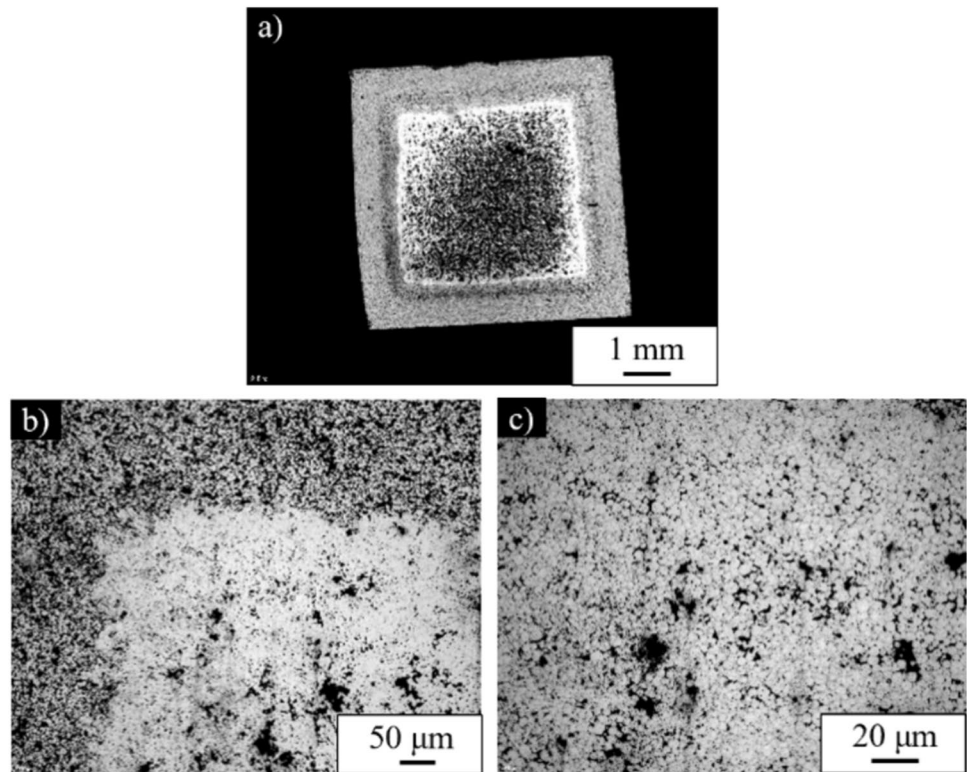
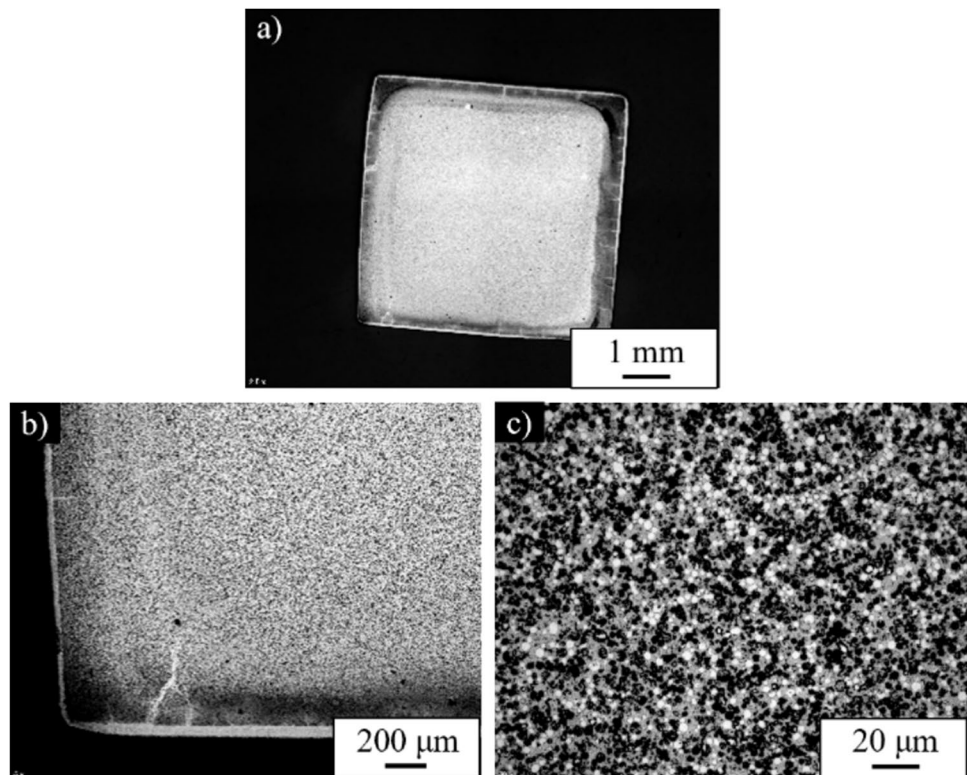


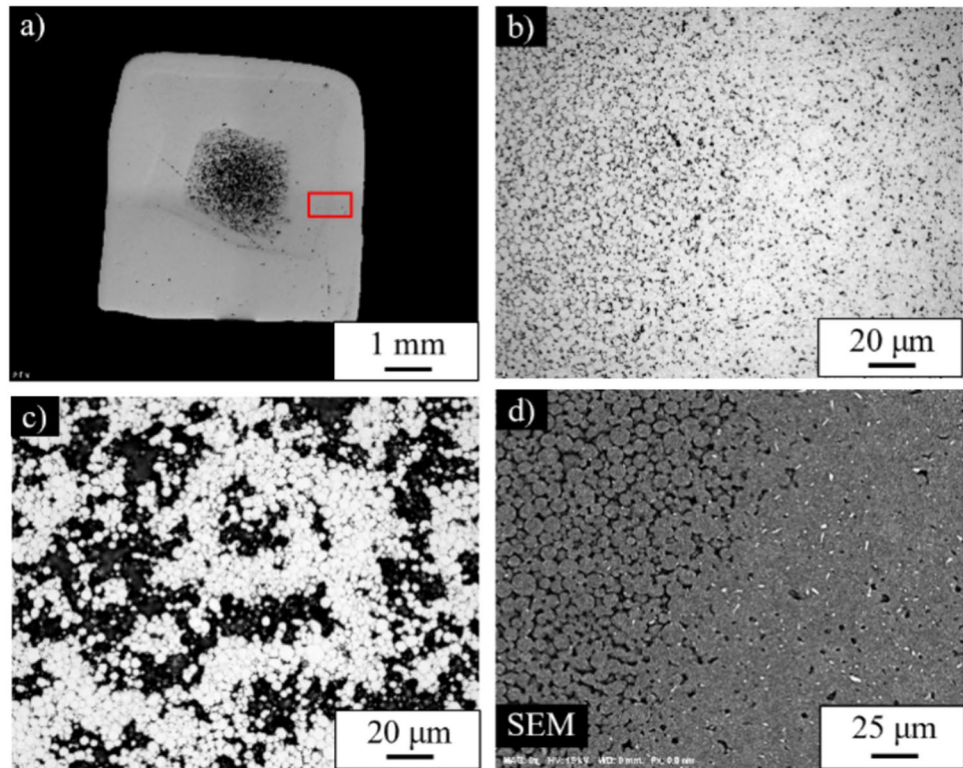
Fig. 7 **a** Microscope overview image of the sintered test specimen C6 (sintered under nitrogen with magnesium addition); **b** detail image of the edge layer; **c** detail image of the inner area



them. Figure 8c shows the core of the sample, where porosities and an initial sintering process can be observed. This suggests that further work should be done on the sintering

parameters. Extending the sintering time could also lead to a complete sintering process in the inner area of specimen D7. When specimens B7 (Fig. 6) and D7 (Fig. 8) are compared,

Fig. 8 **a** Microscope overview image of the sintered test specimen D7 (sintered under argon with magnesium addition) and the framed transition zone; **b** image of the transition zone; **c** image of the inner area; **d** SEM image of the transition zone



the advantage of adding magnesium in the sintering furnace becomes clear: the sintered area in specimen D7 is significantly larger, as the oxygen partial pressure was reduced by the magnesium, allowing sintering to take place even in the outer area of the specimen. Figure 8d) shows a SEM image of the transition zone of sample D7. White needles can be seen in the sintered outer area, which could be an accumulation of aluminum oxide.

Another explanation for these needles could be the accumulation of iron. Iron has been widely recognized as being almost insoluble in aluminum, with a maximum solubility of 0.04%. However, even in small quantities, iron is consistently found in aluminum, as it also can be found in the aluminum powder used, containing 0.12 wt.% iron. It has been observed that during longer annealing times, the presence of iron in aluminum leads to the formation of brittle AlFe needles. [19]

The relative density of the samples A5 and B5 sintered under normal atmosphere and without magnesium addition in the sintering furnace did not show any increase in density, indicating a failed sintering process. This is also evident from the microscope images in Fig. 9a and b. Figure 9b shows the surface layer of sample A5, which is clearly visible in the overview image in a. Although some of the aluminum particles appear to have deformed slightly due to diffusion, no connection between the individual particles (sinter necks) could be observed. Figure 9c shows clearly that no sintering of the material was achieved. This

image also explains why the interior of the sample appears black in Fig. 9a: these are aluminum particles that are located below the ground surface. These appear dark in the microscope image.

Comparing the surface layer of sample A6 in Fig. 5c with the surface layer of sample C6 in Fig. 10, which was sintered under a nitrogen protective gas atmosphere with an addition of magnesium in the sintering furnace, shows that the unsintered surface layer seen in sample A6 is no longer visible in sample C6. The addition of magnesium in the sintering atmosphere may be responsible for this, as it binds the residual oxygen in the sintering atmosphere and thereby minimizes the effect of “self-gettering”. The same applies to the surface layer of sample B7 (Fig. 6) when compared to the surface layer of sample D7 in Fig. 10. Here, the unsintered surface layer has become significantly thinner, measuring only 20 μm in thickness.

By utilizing the atomic weights of elements Al and N or Al and Mg from the periodic table, along with the number of atoms in compounds AlN and Al₃Mg₂, it is possible to estimate the ratio of these compounds in the structure of the sintered body. This estimation is specifically performed for samples sintered solely under nitrogen (A6 and A7) and samples sintered under argon with the addition of magnesium in the sintering furnace (D6 and D7), as these samples exhibited the largest increase in density (Fig. 3). The observed mass increase is solely attributed to the reaction of the respective atmosphere or

Fig. 9 **a** Microscope overview image of the sintered test specimen A5 (sintered under normal atmosphere); **b** image of the outer zone; **c** image from the inner area

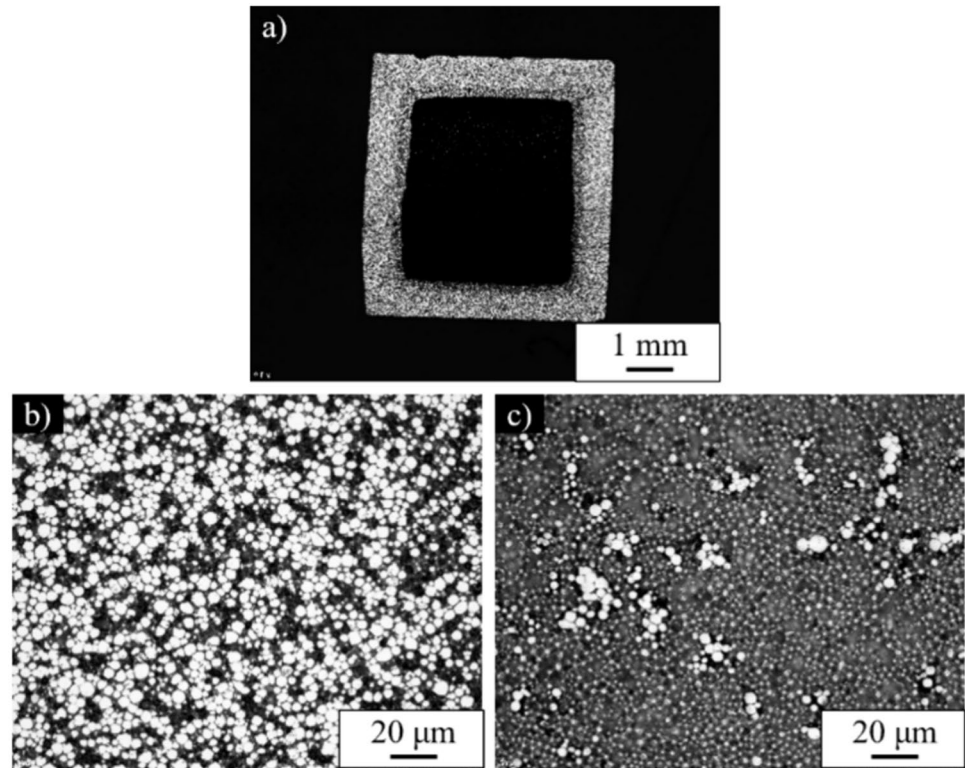


Fig. 10 Micrographs of the surface layers of sample C6 and D7

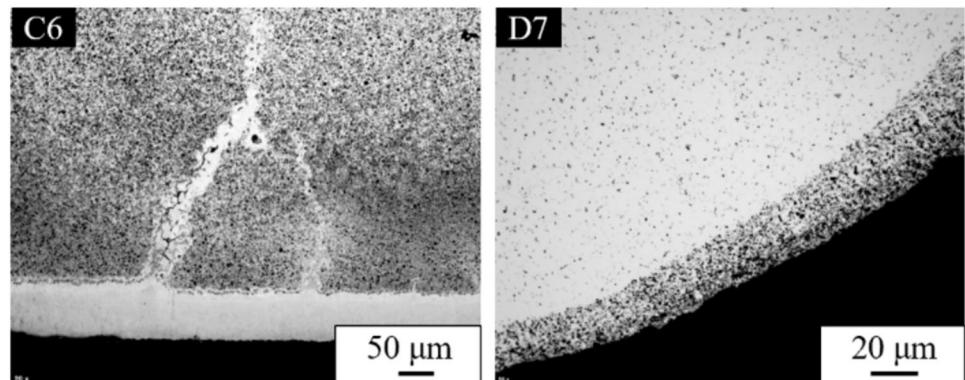


Table 2 Mass proportions of the respective compounds AlN and Al₃Mg₂ in the sintered samples

Sample	Al %	AlN %	Al ₃ Mg ₂ %
A6	64.3	35.7	–
A7	61.3	38.7	–
D6	90.4	–	9.6
D7	91.2	–	8.8

the magnesium additive with the sample. The results can be viewed in Table 2.

The formation of the ceramic AlN, with an average content of 37.2%, is relatively high and considered detrimental

when it comes to the sintering of a metallic component. In contrast, the formation of the metallic compound Al₃Mg₂ is relatively small with an average of 9.2%. This is not a significant issue, as Al₃Mg₂ is also a metallic compound.

4 Conclusion and outlook

The coating parameters used were found to be effective in producing powder compacts with a relative density of 62%, which is sufficient enough for complete compaction and sintering [3, 20]. With powder-based binder jetting using water-atomized pure iron powder, green densities of up to 48.1% have been achieved [21]. The sintering process yielded

different densities depending on the protective gas atmosphere and magnesium addition. The samples sintered under normal atmosphere and without magnesium addition did not increase in density and the sintering process failed. This was evident from the microscope images, which showed no connection between the aluminum particles.

On the other hand, specimens sintered under a nitrogen protective gas atmosphere without any addition of magnesium showed a significant increase in relative density after sintering. The microscope images of these specimens did not show individual aluminum particles, except in the outer shell, which can be attributed to the “self-gettering” effect. The increase in mass suggests another reaction during the sintering process, most likely nitride formation due to the nitrogen sintering atmosphere. The addition of magnesium in the sintering atmosphere minimized the effect of “self-gettering”. These specimens did not show any change in volume but had an increased mass, likely due to nitride formation. The inner area of these samples looked similar to the samples without the addition of magnesium.

The examination of specimens sintered under an argon protective gas atmosphere revealed interesting findings. The clear outer layer observed in specimens sintered without an addition of magnesium in the sintering furnace is likely due to the “self-gettering” effect. The subsequent layer indicates densification and advanced sintering through deformation of the aluminum particles. Porosities were visible inside the sintered specimens. Comparing specimens sintered under an argon protective gas atmosphere with and without magnesium addition, it becomes evident that adding magnesium in the sintering furnace resulted in a larger sintered area, as the reduction of oxygen partial pressure facilitated sintering even in the outer area. The specimens without magnesium addition exhibited shrinkage but no change in mass during the sintering process.

Specimens sintered under an argon atmosphere and with an addition of magnesium exhibited significant shrinkage and a slight increase in mass. The fact that magnesium has dissolved in aluminum appears to be a possible explanation for this. At low temperatures, magnesium exhibits slight solubility in aluminum, with a solubility limit of less than 2% in the α -crystal-phase [19]. However, beyond this solubility limit, a new phase known as the β -phase, specifically AlMg, starts to form. This precipitation of the β -phase occurs primarily at the grain boundaries of the material [19]. The transition area of these specimens showed more advanced density and sintering degree in the outer layer compared to the inner area. Sintering necks were observed in the inner area. Improved sintering parameters, e.g., extending the sintering time or temperature, may lead to complete sintering in the inner area.

Based on the assumption that the formation of AlN or Al₃Mg₂ can occur during sintering, it has been found that

sintering of aluminum under an argon protective gas atmosphere with the addition of magnesium yields a high average aluminum content of 90.8%. On the other hand, sintering under a pure nitrogen atmosphere result in a lower average aluminum content of 62.8%.

These findings provide valuable insights into the nature and material composition of the sintered specimens, highlighting the effects of “self-gettering” and the influence of magnesium addition during the sintering process. Further research and optimization of sintering parameters are recommended for better control and understanding of the sintering process.

It has been shown that only by adding solid magnesium to the sintering atmosphere, sintering of aluminum can be improved substantially, particularly in argon atmosphere. Future investigations will address the optimization of the slurry-based 3D-printing process to enable higher green densities, the adjustment of the sintering curve (i.e., holding times) and the analysis of the mechanical properties. It can be envisaged that by understanding the relation between the 3D-printing process, the sintering parameters, and the formation of the microstructure, the material properties can be predicted or even precisely set.

Acknowledgements The research reported in this article was supported by the Bayerische Forschungsstiftung (grant number AZ-1541-22). The authors sincerely thank the funding authority and the project partners voxeljet AG and Schlenk Metallic Pigments GmbH for their valuable collaboration.

Author contributions Conceptualization: Jan Angenooth, Patricia Erhard, Daniel Günther; methodology: Jan Angenooth, Patricia Erhard; formal analysis and investigation: Jan Angenooth, Dennis Wächter; writing—original draft preparation: Jan Angenooth; writing—review and editing: Patricia Erhard, Daniel Günther; supervision: Daniel Günther, Wolfram Volk.

Funding Open Access funding enabled and organized by Projekt DEAL.

Data availability The data that support the findings of this study are available on request from the corresponding author.

Open Access This article is licensed under a Creative Commons Attribution 4.0 International License, which permits use, sharing, adaptation, distribution and reproduction in any medium or format, as long as you give appropriate credit to the original author(s) and the source, provide a link to the Creative Commons licence, and indicate if changes were made. The images or other third party material in this article are included in the article’s Creative Commons licence, unless indicated otherwise in a credit line to the material. If material is not included in the article’s Creative Commons licence and your intended use is not permitted by statutory regulation or exceeds the permitted use, you will need to obtain permission directly from the copyright holder. To view a copy of this licence, visit <http://creativecommons.org/licenses/by/4.0/>.

References

- Sachs EM, Haggerty MJ, Cima MJ, Williams PA (1989) Three dimensional printing techniques. US5204055A
- Sachs EM, Cima MJ, Caradonna MA, Grau J, Serdy JG, Saxton PC, Uhland SA, Moon J (1998) Patents Jetting layers of powder and the formation of fine powder beds thereby. US6596224B1
- Zocca A, Colombo P, Gomes CM, Günster J (2015) Additive manufacturing of ceramics: issues, potentialities, and opportunities. *J Am Ceram Soc* 98:1983–2001. <https://doi.org/10.1111/jace.13700>
- Zocca A, Lima P, Günster J (2017) LSD-based 3D printing of alumina ceramics. *J Ceram Sci Tech*. <https://doi.org/10.4416/JCST2016-00103>
- Bhuvanesh Kumar M, Sathiya P (2021) Methods and materials for additive manufacturing: a critical review on advancements and challenges. *Thin-Walled Struct*. 159:107228. <https://doi.org/10.1016/j.tws.2020.107228>
- Mostafaei A, Elliott AM, Barnes JE, Li F, Tan W, Cramer CL, Nandwana P, Chmielus M (2021) Binder jet 3D printing—process parameters, materials, properties, modeling, and challenges. *Prog Mater Sci* 119:100707. <https://doi.org/10.1016/j.pmatsci.2020.100707>
- E.M. Sachs, US6036777A—Powder dispensing apparatus using vibration, 2023. <https://patents.google.com/patent/US6036777A/en> (accessed 21 November 2023).
- Zheng J, Reed JS (1989) Effects of particle packing characteristics on solid-state sintering. *J Am Ceram Soc* 72:810–817. <https://doi.org/10.1111/j.1151-2916.1989.tb06222.x>
- Erhard P, Angenoorth J, Vogt J, Spiegel J, Ettetmeyer F, Volk W, Günther D (2021) Characterization of slurry-cast layer compounds for 3D printing of high strength casting cores. *Materials* (Basel). <https://doi.org/10.3390/ma14206149>
- Nylund A, Olefjord I (1993) Surface analysis of air exposed rapidly solidified aluminium powder. *Powder Metall* 36:193–197. <https://doi.org/10.1179/pom.1993.36.3.193>
- Beiss P (2013) *Pulvermetallurgische Fertigungstechnik*. Springer Vieweg, Berlin, Heidelberg
- U. Füssel (2015) Korrelation zwischen der Oberflächenhistorie, den Prozessbedingungen und der Lötbarkeit von Aluminiumwerkstoffen. Schlussbericht, 2015. https://tu-dresden.de/ing/maschinenwesen/if/fue/ressourcen/dateien/ag_thermisches_fuegen/abschlussberichte/IGF17.748_Schlussbericht?lang=de (accessed 22 November 2023).
- Schaffer GB, Hall BJ (2002) The influence of the atmosphere on the sintering of aluminum. *Metall Mater Trans A* 33:3279–3284. <https://doi.org/10.1007/s11661-002-0314-z>
- M. Qian, G.B. Schaffer, *Sintering of aluminium and its alloys, in: Sintering of Advanced Materials*, Elsevier, 2010, pp. 291–323.
- Pieczonka T (2017) Disruption of an alumina layer during sintering of aluminium in nitrogen. *Arch Metall Mater* 62:987–992. <https://doi.org/10.1515/amm-2017-0139>
- MacAskill IA, Hexemer RL, Donaldson IW, Bishop DP (2010) Effects of magnesium, tin and nitrogen on the sintering response of aluminum powder. *J Mater Process Technol* 210:2252–2260. <https://doi.org/10.1016/j.jmatprotec.2010.08.018>
- Rukini A, Rhamdhani MA, Brooks GA, van den Bulck A (2022) Metals production and metal oxides reduction using hydrogen: a review. *J Sustain Metall* 8:1–24. <https://doi.org/10.1007/s40831-021-00486-5>
- T. Pieczonka, S. Schubert, S. Baunack, B. Kieback, *Sintering behaviour of aluminium in different atmospheres*, 2005.
- C. Kammer, *Grundlagen und Werkstoffe, first. überarb. Ausg. der fünfzehnten. Aufl.*, Aluminium-Verlag, Düsseldorf, 1998.
- Lima P, Zocca A, Acchar W, Günster J (2018) 3D printing of porcelain by layerwise slurry deposition. *J Eur Ceram Soc* 38:3395–3400. <https://doi.org/10.1016/j.jeurceramsoc.2018.03.014>
- Rishmawi I, Salarian M, Vlasea M (2018) Tailoring green and sintered density of pure iron parts using binder jetting additive manufacturing. *Addit Manuf* 24:508–520. <https://doi.org/10.1016/j.addma.2018.10.015>

Publisher's Note Springer Nature remains neutral with regard to jurisdictional claims in published maps and institutional affiliations.